Radiation Physics and Chemistry 238 (2026) 113170

Contents lists available at ScienceDirect

Radiation Physics and Chemistry

journal homepage: www.elsevier.com/locate/radphyschem

A novel PSQA brain phantom using G-GAAB gel to measure non-coplanar dose with IMRT and VMAT techniques in radiation therapy

Niju Thankachan T [a,b], Sreelakshmi K.[a], Nirmala R. James [c], Jojo P. John [d], B.R. Bijini [b,e,*]

[a] Department of Radiation Oncology, Government Medical College, Thiruvananthapuram, Kerala, India
[b] PG Department and Research Centre in Physics, Mahatma Gandhi College, University of Kerala, India
[c] Department of Chemistry, Indian Institute of Space Science and Technology, Thiruvananthapuram, Kerala, India
[d] School of Applied Physics, Papua New Guinea University of Technology, Morobe, Lae, 411, Papua New Guinea
[e] Department of Physics, VTMNSS College, University of Kerala, Thiruvananthapuram, Kerala, India

ARTICLE INFO

Handling Editor: Dr. Chris Chantler

Keywords:
G-GAAB gel
PSQA
Point dose measurement
Gamma index evaluation
Radiation detectors
Brain

ABSTRACT

Bovine gelatin in gum arabic aldehyde as cross-linking agent in borax (G-GAAB gel) is a newly developed brain phantom for radiation dosimetry. Evaluation of 3-dimensional dose (3D) distribution in G-GAAB gel and non-coplanar dose measurement will help to understand the energy deposition of radiation inside the gel volume. Aim of this study is to analyse the 3D dose distribution, non-coplanar point dose measurement in G-GAAB gel using various detectors and to verify whether G-GAAB gel to be used as a new patient specific quality assurance (PSQA) brain phantom for intensity modulated radiation therapy (IMRT) and volumetric modulated arc therapy (VMAT) techniques in radiation therapy. G-GAAB gel phantom was made inside a perspex box and radiation detectors at multiple planes were inserted. Imaging, contouring, planning with Treatment Planning System (TPS), plan evaluation by different methods, PSQA, verification of 3D distribution and point dose measurement was performed with various treatment techniques. 30 different retrospective brain tumour cases were taken for creating verification plan in G-GAAB gel using IMRT and VMAT. Standard deviation, for 0.6cc FC (FC), 0.65cc FC and Semiflex chamber, was 0.825, 0.803 and 0.889 respectively in G-GAAB gel. Measured P-value for ionization chamber dose readings inside G-GAAB gel was 0.975, 0.976 and 0.984 for 0.6cc FC, 0.65cc FC and Semiflex chamber respectively which resulted in no significant variation between TPS dose and that delivered. Hence, apart from the radiation properties similar to the brain tissue, 3D dose distribution and non-coplanar point dose measurement also suggest that, G-GAAB gel is a very good substitute for brain tissue. The standard deviation and P-value obtained from this study proved that, G-GAAB gel can be considered as new brain phantom for PSQA in radiation dosimetry for IMRT and VMAT.

1. Introduction

In radiation therapy, establishment of radiation beam data has to be performed prior to actual treatment (Ximenes R.E. et al., 2015). X-ray photon interaction with matter results in deposition of radiation absorbed dose into the depth. For radiation treatments, the depth dose distribution and hence the dose delivery must be precise. Usually, a phantom composed of tissue-equivalent material is used for such measurements, with water being universally considered as the gold standard (C.C. Ferreira et al., 2010). Gel materials have been explored as suitable phantom materials for brain tissue due to their physical nature (Prabhu S. et al., 2021). For applications involving high-energy radiation, the physical and radiological characteristics of the phantom material must closely resemble those of biological tissues (Yohannes et al., 2012).

Many of the currently available commercial patient specific quality assurance (PSQA) phantoms, including the in-built Electronic Portal Imaging Device (EPID) of Linear Accelerators (Linac) are rigid and predominantly designed for coplanar radiation verification using flat-panel detectors (James et al., 2023; Miri et al., 2016; Shi et al., 2019). These phantoms, due to the rigid nature, typically lack geometrical and anatomical adaptableness to accurately represent brain tissues for such configurations and are usually not flexible in physical properties (Rousseau et al., 2023; Nur Emirah Mohd Zain et al., 2019). Even though the available PSQA phantoms are useful for dose verification prior to treatment using Intensity Modulated Radiation Therapy (IMRT), cost and limited measurement options are highlighted as limitations (Kumar

* Corresponding author. Department of Physics, VTM NSS College, Thiruvananthapuram, Kerala, India.
E-mail address: bijinijyothis1@gmail.com (B.R. Bijini).

https://doi.org/10.1016/j.radphyschem.2025.113170
Received 13 March 2025; Received in revised form 26 June 2025; Accepted 9 July 2025
Available online 11 July 2025

et al., 2009). Synthetic phantoms, which are considered as good option for training, research and in computer aided surgery, find difficult to replicate for complex organs like the brain (Forte et al., 2016). Non-coplanar techniques like IMRT and Volumetric Modulated Arc Therapy (VMAT) use beam arrangements involving oblique or non-coplanar angles to spare critical structures in the brain. The positioning of detectors in multiple planes is still a challenge for commercial phantoms to evaluate comprehensive patient-specific QA in complex techniques like IMRT and VMAT (SlobodanDevic, 2011). The plastic-based phantoms which are commonly used for dosimetric analysis may not precisely exhibit the radiological attenuation and dose distribution characteristics of brain tissue, especially for multiple plane beam arrangements (Andrea Molineu et al., 2005). Despite advancements, many of these phantoms are limited in their ability to replicate the brain tissue measurements to specific planes (Tino, R et al., 2019). Their geometric configurations limit their adaptability for dose measurements in non-coplanar setups commonly used in advanced radiotherapy techniques like IMRT and VMAT (Kruszyna-Mochalska, M et al., 2022, Miften, M et al., 2018, Low, D. A et al., 2011) Moreover, rigid phantoms may not account for the dose variations arising from non-coplanar field arrangements, which may lead to inaccuracy in dose verification. Therefore, achieving accurate non-coplanar point dose measurements remains a challenge with existing commercial phantoms. This necessitates the development of a gel-based brain equivalent phantom with anatomically relevant, brain tissue-equivalent, enhanced adaptability and flexibility capable of measuring non-coplanar for three-dimensional dose verification.

To address these limitations, we introduce a novel PSQA phantom developed using gelatin crosslinked with gum arabic aldehyde in borax (G-GAAB gel). Unlike conventional rigid phantoms, G-GAAB gel exhibits radiological properties closely matching those of brain tissue while also allowing detectors to be positioned at any desired location and directions within the phantom volume, including non-coplanar geometries. Our previous study confirmed the suitability of G-GAAB gel as a brain tissue-equivalent material in terms of radiation absorption, scattering, CT number, density, stability, and dosimetric accuracy (T. Niju Thankachan et al., 2025), where depth dose was studied along the central axis using dual-energy X-ray photons. However, beyond central axis dosimetry, three-dimensional (3D) volumetric dose distribution, its evaluation, and non-coplanar point dose measurements inside G-GAAB gel need to be studied to assess energy deposition comprehensively throughout the phantom. Given that G-GAAB gel mimics brain tissue radiation interaction properties and enables dose measurement at any plane or position, this study investigates its potential as a novel PSQA phantom for dose measurements in advanced radiotherapy techniques like IMRT and VMAT.

Photon interaction characteristics in phantom materials must be comparable to human tissues (Fisher R. & Hintenlang D., 2006), and the evaluation of absorbed energy per unit mass is essential (Marashdeh M. & Abdulkarim M., 2023; H. Sekkat et al., 2025). Studying volumetric dose deposition in brain-equivalent phantoms is particularly relevant given the increasing incidence of brain tumours globally (Grech N. et al., 2020; Irena Ilic and Milena Ilic, 2023). Precise dose distribution is essential for maximizing tumour control while sparing normal tissues (Sebastiaan Breedveld et al., 2019), and treatment plans generated by the TPS must be evaluated to ensure optimal delivery (Victor Hernandez et al., 2020). Plan verification based on Dose Volume Histogram (DVH) enhances the quality assurance process by improving the understanding of dose uncertainty (Visser R. et al., 2014).

The precision of dose delivery to the planning target volume (PTV), while sparing surrounding normal tissues, can be quantitatively assessed using the Conformity Index (CI) (Paddick I., 2000; Sinead M. et al., 2010). Ideal conformity is achieved with CI values approaching 1. Additionally, homogeneity of dose distribution is an important parameter measured by the Homogeneity Index (HI) (Kataria T. et al., 2012), with values close to zero indicating better uniformity and reduced risk of hot and cold spots (Kyei K.A. et al., 2024; Petrova D. et al., 2017).

Point dose measurements are equally significant for verifying doses delivered to specific locations within target volumes or surrounding healthy tissues. Such measurements are an effective tool in PSQA for IMRT to confirm dose accuracy (Kumar A. et al., 2007). Chambers calibrated by secondary standard calibration laboratories are used for absolute point dose measurements (Mahmood T. et al., 2017), typically performed in homogeneous phantoms (Singh S. et al., 2019). Since G-GAAB gel exhibits homogeneous density equivalent to that of brain tissue (T. Niju Thankachan et al., 2025), it is well suited for accurate point dose verification, including in non-coplanar geometries.

PSQA is crucial for IMRT and VMAT to verify that TPS-generated dose distributions match delivered doses (Agazaryan N. et al., 2003; Menzel H.G., 2010). Verification processes include point dose measurements using ionization chambers, 2D/3D film dosimetry, detector arrays, and EPID-based portal dosimetry with gamma index analysis (Nishiyama S. & Takemura A., 2023; Nasseri S. et al., 2022). Most currently used PSQA phantoms, however, remain restricted to coplanar or planar dose verification, emphasizing the importance of a phantom like G-GAAB gel, which allows dose verification at arbitrary, including non-coplanar, points.

Linear accelerators generate therapeutic X-ray beams by accelerating electrons via high-frequency electromagnetic waves and striking a metallic target (Khan F.M. & Gibbons, 2014). In this study, various angled radiation beams were used with IMRT and VMAT, with detectors aligned in non-coplanar inside the G-GAAB gel phantom to verify complex dose distributions.

2. Materials and methods

Bovine gelatin (Type B) and gum arabic for preparing G-GAAB gel were procured from M/s SRL chemicals and M/s ISOCHEM respectively. Acetic acid was obtained from M/s Sigma Aldrich. Experimental setup, for measuring and analyzing the volumetric dose distribution inside G-GAAB gel, was prepared using a perspex made rectangular box of dimension 20cm x 15cm x 15cm. G-GAAB gel was filled inside the box. Provisions for inserting radiation detectors were made at the sides of the perspex box. One chamber was positioned directly in the centre of the setup and can be aligned with the central axis of the beam. Other detectors were placed in a non-coplanar manner in the G-GAAB gel phantom. The radiation detectors used in this study were 0.6cc Farmer Chamber (FC), 0.07cc Semiflex field chamber, 0.07cc Semiflex reference chamber, 0.016cc pin point chamber, 0.03cc micro silicon and 0.03cc diode p detector. Charge due to ionization in the chamber volume was measured using an Unidos E Electrometer. All the detectors and the electrometer were PTW, Germany made. Another 0.65cc FC (Rosalina) was also used with Standard Imaging Supermax Electrometer. All the detectors were calibrated in secondary standard laboratory.

2.1. G-GAAB gel fabrication

G-GAAB gel was prepared with gelatin (type B) and oxidized gum arabic in borax solution, and performed characterization and radiation dosimetric studies in therapeutic energy range as in (T. Niju Thankachan et al., 2025). The elemental constituents, percentage elemental composition and the basic concentration used for G-GAAB gel preparation was mentioned in Table 1, Tables 2 and 3 respectively.

Fourier Transform InfraRed (FTIR) spectroscopy analysis of G-GAAB gel confirmed successful oxidation of gum arabic, with the appearance of a characteristic aldehyde carbonyl peak at 1726cm^{-1}. Using 14% oxidized gum arabic as the cross-linking agent resulted in a stable gel with a measured density of 1.034g/cm^3, closely matching the density of brain tissue (1.04g/cm^3, ICRU Report 44). CT analysis showed only a 2% variation in CT numbers compared to brain, with mean CT values of 37.44 ± 12.09HU for G-GAAB gel and 31.32 ± 17.59HU for a brain-equivalent phantom insert. From the experimental measurements of

Table 1
Elemental constituents of G-GAAB gel.

Sl. No	Composition of G-GAAB gel	Elemental constituents
1	Bovine Gelatin- Type of protein material extracted from collagen of bovine	Carbon, Hydrogen, Oxygen and Nitrogen.
2	Gum Arabic Aldehyde – Polysaccharide extracted from Gum Acacia	Carbon, Hydrogen, Oxygen and less amount of nitrogen
3	Borax	Sodium, Boron, Oxygen and Hydrogen
4	Water	Hydrogen and Oxygen

Table 2
Percentage elemental composition of G-GAAB gel.

Element	percentage by mass of G-GAAB gel
Carbon	43.8%
Hydrogen	6.5%
Oxygen	36%
Nitrogen	11.3%
Sodium	1.2%
Boron	1.2%

Table 3
Basic concentrations of Components used in the preparation of G-GAAB gel.

Constituents of G-GAAB gel	Concentration
Gelatin	25% w/v
Gum arabic aldehyde (cross linking agent)	10% w/v
Borax (Provides alkaline pH and enhance cross-linking reaction resulting in swift gelation)	0.1M

linear and mass attenuation coefficients using narrow beam geometry with Co-60 and dual-energy X-rays (Thankachan et al., 2025), calculated mass attenuation coefficients (MAC) of G-GAAB gel at 1.25MeV, 6MV, and 15MV showed excellent agreement with those of brain tissue (ICRU 44), with percentage deviations of 0.31%, 0.36%, and 1.04%, respectively. Depth dose measurements in the G-GAAB gel phantom under various setup conditions demonstrated a linear correlation with reference measurements obtained from a standard Radiation Field Analyser (RFA) water phantom and a commercial beam quality index phantom, with dose deviations within 2%. The gel also exhibited good stability, maintaining its structural integrity for up to one month at room temperature without refrigeration, even after repeated exposures to high-energy X-rays and gamma rays. These results confirm that G-GAAB gel exhibits radiation attenuation characteristics similar to brain across clinical therapeutic photon energies. Beyond a period of one month from the preparation of G-GAAB gel, partial loss of viscosity was observed at room temperature (28–30°C), while slight shrinkage and hardening occurred at 23°C due to water loss.

2.2. Simulation and delineation

Lead fiducial markers were aligned with the external moving lasers (Gammex) positioned on the surface of the Perspex box. The G-GAAB gel, with all detectors in place inside the Perspex box, was then scanned using a CT simulator (Discovery RT, GE Healthcare) at 120kVp. (Mahur et al., 2017). Scanned images were transferred to the server system of Linear accelerator. Delineation of the image sets was performed using the contouring workstation (Varian Somavision). All detectors embedded within the G-GAAB gel were contoured as individual structures. Two of these structures were designated as PTVs, named PTV High A and PTV Intermediate B, while the remaining five detectors were considered as Organs at Risk (OARs) and labelled OAR C, OAR D, OAR E, OAR F, and OAR G. To better simulate actual clinical PTV and OAR structures, the detectors were contoured irregularly with an outer margin of 2.5cm–3.5cm. For the detectors designated as PTVs, the volume of the reference chamber was specifically contoured as the Gross Tumour Volume (GTV). A Simultaneous Integrated Boost (SIB) technique was planned to deliver 66Gy to PTV High A and 60Gy to PTV Intermediate B (Salam Abdulrazzaq Ibrahim Al-Rawi Hassan Abouelenein Magdy Mohammed Khalil, 2022). All other detectors were considered as OARs and appropriate dose-volume constraints were applied during treatment planning.

2.3. Treatment planning

Subsequent treatment planning for the G-GAAB gel phantom was carried out using the contoured images in the TPS (Varian Eclipse 16.1). Two plans were generated: one using IMRT with seven radiation beams and the other using VMAT with two arcs. Irradiation was planned with 6MV X-ray photons. Both IMRT and VMAT plans were optimized to achieve the prescribed PTV doses while meeting the defined dose-volume constraints for OARs (Wilko F.A.R et al., 2009). During optimization, priority was given to ensure 100% of the GTV received 100% of the prescribed dose, with at least 95% dose coverage to 100% of the PTV volume. The maximum dose was constrained to remain below 107% of the prescribed dose (Knöös, T et al., 1998), while also meeting the dose constraints for normal structures. The approved treatment plans were then exported to the linear accelerator (Varian Clinac-iX) for irradiation of the G-GAAB gel phantom.

2.4. Plan evaluation

Volumetric dose coverage of the GTV, PTV, and OARs was evaluated using the 3-dimensional distribution of isodose lines. The DVH provided a graphical summary of the radiation dose distribution within the target volumes and OARs. (Drzymala, R. E et al., 1991). This evaluation helps assess the effectiveness of the treatment plan. The cumulative DVHs of both IMRT and VMAT plans were used to evaluate and compare the dose delivered to the PTV between the planned and executed treatments. Key dosimetric parameters such as the dose received by 95% of the PTV volume ($D_{95\%}$), maximum dose (D_{max}), mean dose (D_{mean}), and the volume of PTV receiving 95% of the prescribed dose ($V_{95\%}$) were extracted from the DVHs for analysis.

Conformity Index was used to assess the degree of conformity between the prescribed radiation dose and the target volume (Kyei, K. A et al., 2024) and is represented in Formula 1

$$CI = \frac{V_{95}}{V_{PTV}} \tag{1}$$

where, V_{95} is the volume covering 95 % isodose and V_{PTV} is volume of PTV

Homogeneity Index was used to evaluate the uniformity of the radiation dose distribution within the target volume (Kyei, K. A et al., 2024) and represented as in Formula 2

$$HI = \frac{D_{2\%} - D_{98\%}}{D_{50\%}} \tag{2}$$

where, $D_{2\%}$ is the dose received by 2% of the PTV, $D_{98\%}$ is the dose received by 98% of PTV and $D_{50\%}$ is the dose received by 50% of the PTV

2.5. Setup fields and DRR

The isocentre of the generated plan was positioned within the PTV, and Digitally Reconstructed Radiograph (DRR) images were generated for each beam. The shift of the isocentre from the user-defined origin was measured, and three setup fields with corresponding DRRs were included to assist in aligning the G-GAAB gel phantom during treatment setup. Two setup fields were acquired using the kV X-ray source of the On-Board Imaging (OBI) system at static gantry angles of 0° and 270°,

while Cone Beam CT (CBCT) was performed with a rotating kV source from 22° to 181°. The OBI images were compared with the plan's DRRs to determine the required vertical, longitudinal, and lateral shifts. These calculated shifts were applied to finalize the G-GAAB gel phantom positioning in the treatment unit for irradiation.

2.6. Point Dose measurement

A 3-Dimensional Conformal Radiotherapy (3DCRT) plan was generated in the TPS using CT images to deliver a dose of 5Gy to the G-GAAB gel phantom. A field size of 20cm x 15cm was set to encompass the entire phantom. The reference point was positioned at the centre of the phantom, aligned with the 0.6cc FC placed along the central axis at a depth of 5cm, and the dose was normalized to this point. The 3DCRT plans were created using 6MV X-rays. Point dose measurements provide the absolute dose at the chamber's reference point (Goodwin, D, 2017). In this study, detectors were embedded within the G-GAAB gel phantom at multiple planes to measure absolute dose during irradiation with a linac.

For non-coplanar dose measurements, five ionization chambers and two semiconductor detectors were positioned at predefined locations within the entire volume of the G-GAAB gel phantom. Four detectors (one 0.65cc FC, one 0.6cc FC, one Semiflex chamber, and one Diode-P detector) were inserted from side A of the phantom, while three detectors (one Pin Point chamber, one Semiflex chamber, and one micro silicon detector) were positioned from side B. The two FCs were aligned along the beam's central axis at depths of 5cm and 10cm. The remaining five detectors were positioned off-axis at various depths to assess dose variations across multiple planes. Detector positions were carefully chosen to evaluate central, near-central, and peripheral dose responses for 3DCRT, IMRT, and VMAT deliveries. Specific placements included a Semiflex chamber (8.5cm, side A), Diode-P (12cm, side A), Semiflex (11cm, side B), Pin Point (7.5cm, side B), and micro silicon detector (9cm, side B). The method of aligning detectors in multiple non-coplanar planes inside the gel phantom was shown in Fig. 1a and b and schematic diagram of detector positioning was shown in Fig. 1b.

Non-coplanar point dose calculations were performed for each detector using the Eclipse TPS, with the measurement point fixed at the reference point of each chamber. The finalized treatment plan was then exported to the linac for experimental dose delivery. The G-GAAB gel phantom was irradiated using 6MV X-rays, and point dose measurements from all detectors were recorded using an electrometer. (IAEA TRS 398 rev-1, 2023). Specifications and Calibration factors of each detector were mentioned in Table 4.

The 0.6cc FC (PTW 30013) was calibrated at the Secondary Standard Dosimetry Laboratory (SSDL), Bhabha Atomic Research Centre (BARC), Mumbai, India, along with the electrometer (PTW Unidos E) to ensure consistency. The value of absorbed dose to water calibration factor ($N_{D,W}$) was 5.421 × 10^7Gy/C for Co-60 reference conditions (10 × 10cm^2 field, 80cm SSD, 5cm depth). The absorbed dose to water (D_w) was calculated using Formula 3.

$$D_w = M.\ N_{D,W}.K_{TP}.K_s.K_{pol}.K_{elec}.K_{Q,Q_0} \quad (3)$$

where M is the electrometer reading. Standard correction factor for K_{Q,Q_0} recommended by IAEA TRS-398 Rev.1 was applied for measurements using 0.6cc FC.

K_{Q,Q_0} = 0.991 (6MV), Correction factors during the measurements were, K_{TP} = 0.9987, K_{pol} = 0.9999, K_s = 1.0019 (two-voltage method), and K_{elec} = 1. Detector-specific calibration factors and all corresponding corrections were applied for all detectors used for this study for absorbed dose calculations in 3DCRT, IMRT, and VMAT measurements using the G-GAAB gel phantom.

Point doses calculated from the TPS plan were compared with the corresponding measured doses from the delivered IMRT and VMAT plans, using 6MV photons with a prescribed dose of 5Gy. In this study, non-coplanar point dose measurements were evaluated in the G-GAAB gel phantom using 3DCRT, IMRT, and VMAT techniques with 6MV X-ray photons, delivering a dose of 5Gy. For 3DCRT, a large field size of 20cm x 15cm was selected to match the phantom's dimensions (20cm x 15cm x 15cm), ensuring uniform dose coverage and minimizing heterogeneity. For IMRT and VMAT, field sizes were optimized by the TPS to deliver 5Gy to one detector designated and contoured as PTV high, approximating the phantom's dimensions for adequate target coverage. The use of 6MV photons was appropriate for intracranial irradiation due to their clinical relevance for small to medium target volumes, improved dose conformity, and negligible neutron contamination. A prescription dose of 5Gy was chosen to ensure measurement reproducibility and detector response linearity, balancing the need to avoid both measurement uncertainties at low doses and saturation effects at higher doses.

2.7. Patient specific quality assurance

PSQA is a critical step to ensure that the planned dose in the TPS is accurately transferred to the linear accelerator and precisely delivered during treatment. It is an essential process before clinical implementation to verify that the planned dose corresponds to the delivered dose (Agazaryan, N et al., 2003). Three-dimensional dose verification of the planned treatment was performed using the EPID with the portal dosimetry system. EPID-based portal dosimetry serves as an effective tool for verifying the dosimetric accuracy of planned treatments. (S. Nasseri et al., 2022). The comparison between the measured and planned doses was carried out using gamma index analysis, performed using acceptance criteria set at a dose difference of ≤3% and a distance-to-agreement (DTA) of ≤3mm. A pass rate of area gamma ≥95% was used as the threshold for plan acceptability, in accordance

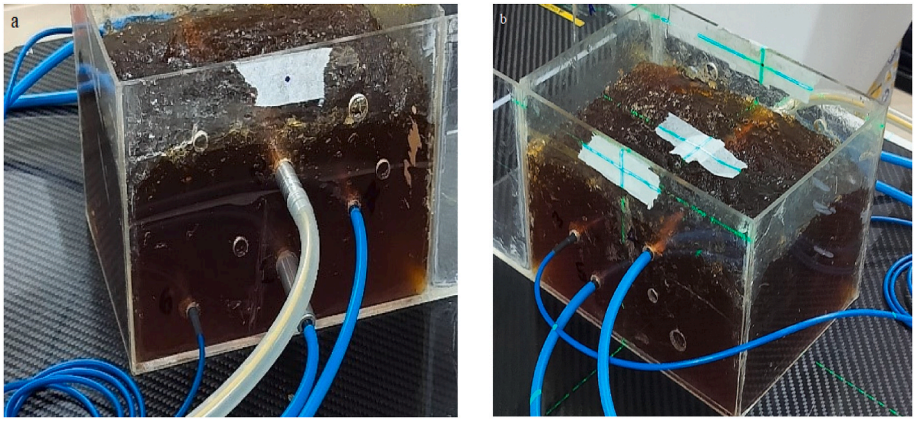

Fig. 1. Detectors positioning inside G-GAAB gel (**a**) Four Detectors in side A (**b**) Three Detectors in side B.

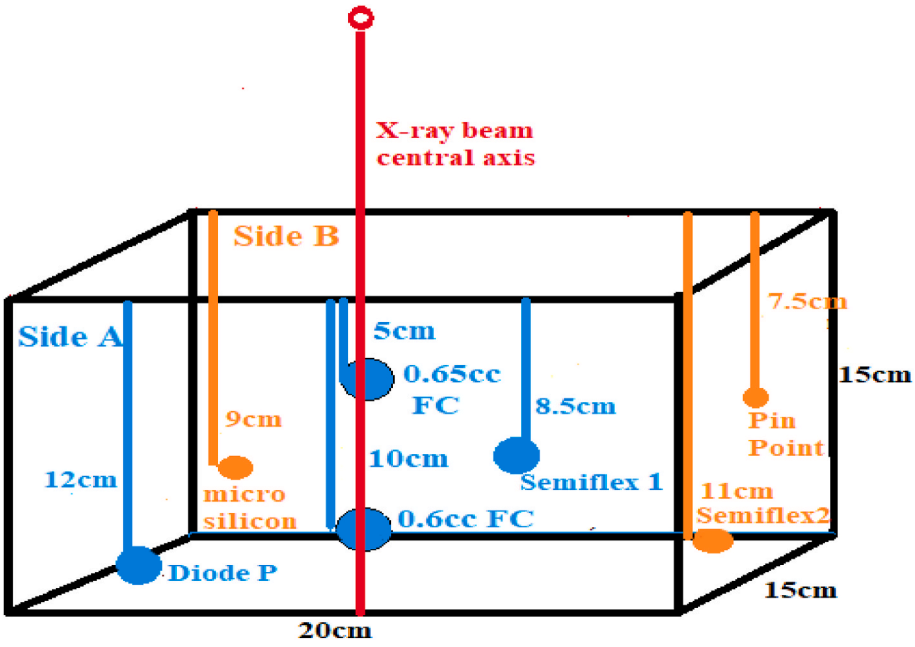

Fig. 1b. Schematic diagram for positioning of seven detectors in G-GAAB gel: 4 detectors from side A (Blue) and 3 detectors from opposite side B (Orange).

Table 4
Detector specifications and calibration details for absorbed dose measurements.

Detector	Type	Nominal sensitive volume	Chamber voltage	Calibration Factor
0.6cc FC (PTW)	Vented cylindrical Ionization chamber	0.6cc	+400V	5.421×10^{7}Gy/C
0.65cc FC (Rosalina)	Ionization chamber	0.65cc	+300V	4.324×10^{7}Gy/C
Semiflex 1 (PTW)	Vented cylindrical Ionization chamber	0.07cc	+400V	5.787×10^{8}Gy/C
Semiflex 2 (PTW)	Vented cylindrical Ionization chamber	0.07cc	+400V	5.811×10^{8}Gy/C
Pin point (PTW)	Vented cylindrical Ionization chamber	0.016cc	+200V	2.437×10^{9}Gy/C
micro silicon (PTW)	Semi-conductor	0.03cc	0V	1.87×10^{-8}C/Gy
Diode P (PTW)	Semi-conductor	0.03cc	0V	9.32×10^{-9}C/Gy

with widely accepted standards for PSQA in external beam radiotherapy. Verification plans for both IMRT and VMAT were generated in the TPS using the actual image series from the treatment plan. These approved verification plans were exported to the Linac, delivered with 6MV X-rays, and captured using the EPID. The delivered dose distributions were then analysed using the portal dosimetry system, and the gamma index was evaluated to assess agreement.

2.8. G-GAAB gel as new PSQA phantom

CT image series of the G-GAAB gel phantom were acquired using a CT simulator with fiducial markers and three ionization chambers (0.6cc FC [PTW], 0.65cc FC [Rosalina], and 0.07cc Semiflex chamber [PTW]) positioned in multiple planes. A new structure set was created in the TPS based on these images, with the active volumes of the chambers contoured. The 0.6cc FC (PTW) was positioned at the centre of the phantom, and the isocentre was set at its reference point.

Image sets of 30 different brain tumour cases, including astrocytoma, glioblastoma, oligodendroglioma, meningioma, and gliomas (six cases each), were retrospectively selected for PSQA. For each case, two verification plans were generated in the TPS, one mapped to the G-GAAB gel phantom and another to a solid slab phantom. Dose from each plan was measured in G-GAAB gel phantom created for PSQA using TPS and calculated the dose in the three chambers. Since the slab phantom is rectangular, perpendicular composite method was adopted for the measurements by making gantry angle zero for all beams by (M. P. Arun Krishnan & M. Ummal Momeen, 2024). To closely replicate the actual treatment delivery conditions, the entire setup of the G-GAAB gel phantom with embedded ionization chambers was irradiated in the linac using the true composite method across 30 verification plans and the absorbed dose was measured using three ionization chambers placed within the gel. A comprehensive comparison was performed between the TPS-calculated dose in the G-GAAB gel and experimentally measured dose in the gel using ionization chambers. Similarly, with the TPS-calculated dose in a slab phantom, and the corresponding measured dose in the slab phantom. This was performed to verify the suitability of the G-GAAB gel phantom as a new PSQA phantom for brain dosimetry in radiation therapy.

For all the techniques, two independent groups were compared: the TPS-calculated dose and the experimentally measured dose. Student's *t*-test (two-sample assuming equal variances) was used to determine the statistical significance of differences between these groups.

3. Results and discussion

In this study, the volumetric dose distribution in G-GAAB gel was evaluated using isodose distributions, DVH, CI and HI. Point dose measurements were performed within the G-GAAB gel for 3DCRT, IMRT, and VMAT plans and compared with corresponding detector-based measurements obtained experimentally using 6MV X-rays. To assess the precision and accuracy of dose delivery using radiation fluence, PSQA was performed with EPID-based portal dosimetry and gamma index evaluation. Verification plans were generated in both G-GAAB gel phantom and slab phantom using 30 retrospective brain

tumour cases to evaluate the suitability of G-GAAB gel as a novel phantom for PSQA.

3.1. Evaluation of TPS plan

3.1.1. Isodose distribution

Two new plans were created in the TPS under a single course, one using seven-field IMRT and the other using VMAT with a single isocentre and two full rotational arcs. Planning priorities for both techniques were set to achieve 95% coverage of the PTV while restricting the maximum dose to within 107% of the prescribed dose. VMAT planning incorporated continuous gantry rotation (181°–179° CW and 179°–181° CCW) with variable gantry speed, dose rates, and dynamic MLC motion. Plan evaluation was carried out using four different methods.

Isodose distribution verification was performed as the first method of plan evaluation. It was observed that 100% of the PTV-high volume received more than 95% of the prescribed 66Gy dose (62.7Gy), and 100% of the PTV-intermediate was similarly covered with over 95% of the prescribed 60Gy dose (57Gy). All OARs received doses well within the prescribed clinical constraints ($D_{max} < 54$Gy, $D_{max} < 10$Gy, $D_{mean} < 26$Gy, $D_{mean} < 35$Gy), ensuring adherence to standard dose limits typically applied in head and neck tumours in radiotherapy.

3.1.2. DVH analysis

The second method of plan evaluation was carried out using cumulative DVH analysis. In the DVH, the relative percentage dose (%) was plotted on the X-axis and the percentage of the total structure volume on the Y-axis. The cumulative DVH graphs for the IMRT and VMAT plans are presented in Fig. 2a and b, respectively.

From the DVH analysis, it was observed that both PTV High and PTV Intermediate achieved coverage of more than 95% of their respective prescribed doses of 66Gy and 60Gy. The 3D maximum dose to PTV High was 104.5% with IMRT and 106.2% with VMAT, while for PTV Intermediate, the 3D maximum dose was 103.3% with IMRT and 96.1% with VMAT. The doses to the OARs were minimal and remained well within the prescribed constraints.

3.1.3. CI and HI

CI and HI measurements were used as the third technique for plan evaluation. The CI, representing the dose coverage of the PTV, was calculated using Formula 2. For the IMRT plan, the volume receiving 95% of the prescribed dose ($V_{95\%}$) was 76.033 cm^3, while the volume of the PTV (V_{PTV}) was 76.13cm^3, resulting in a CI of 0.9987. For the VMAT plan, $V_{95\%}$ was 76.076cm^3, and the calculated CI was 0.9992. The CI values, being very close to 1 for both IMRT and VMAT, indicated excellent conformity and uniform dose coverage within the G-GAAB gel phantom. The HI was calculated using Formula 3 to assess the uniformity of dose distribution within the PTV. For the IMRT plan, the doses received by 2 %, 50%, and 98% of the target volume ($D_{2\%}$, $D_{50\%}$, and $D_{98\%}$) were 67.199Gy, 65.499Gy, and 64.32Gy, respectively. For the VMAT plan, the corresponding values were 67.153Gy, 66.118Gy, and 64.874Gy. The calculated HI values were 0.0439 for IMRT and 0.0344 for VMAT. These HI values, being close to zero, indicated a uniform and homogeneous dose distribution within the G-GAAB gel for both techniques. From the results, the CI values being close to 1 and the HI values approaching zero indicated that both IMRT and VMAT plans achieved excellent dose conformity and uniformity within the G-GAAB gel phantom.

3.2. Non-coplanar point dose

The point doses from each chamber were determined from electrometer readings in nano coulombs (*nC*), applying appropriate calibration and correction factors. (IAEA TRS 398 rev-1).

Point dose calculations were also performed in Eclipse TPS for the IMRT and VMAT plans prescribed with 5Gy to PTV High. For the IMRT plan, point doses were calculated for all detectors across the seven individual radiation beams, while for the VMAT plan, point doses were obtained for the two arc beams. Both plans were exported to the Linac system, and irradiation was carried out using 6MV photons. Experimental point dose measurements were recorded for each beam in both IMRT and VMAT deliveries. The measured doses were then compared with the corresponding TPS-calculated doses to evaluate the agreement between the planned and delivered treatments.

A comparison of non-coplanar point dose measurements, for a prescribed dose of 5Gy, between the TPS-generated plans and experimentally delivered plans for 3DCRT, IMRT, and VMAT techniques using 6MV photons across all chambers is presented in Table 5. A summary of percentage dose deviations for all three techniques and detectors is provided in Table 6.

The results showed that for 3DCRT, the dose received by the 0.6cc FC was 4.997Gy in the TPS plan and 4.961Gy from experimental measurement, corresponding to a deviation of −0.72%. For IMRT, the respective doses were 5.022Gy (TPS) and 5.048Gy (measured), with a

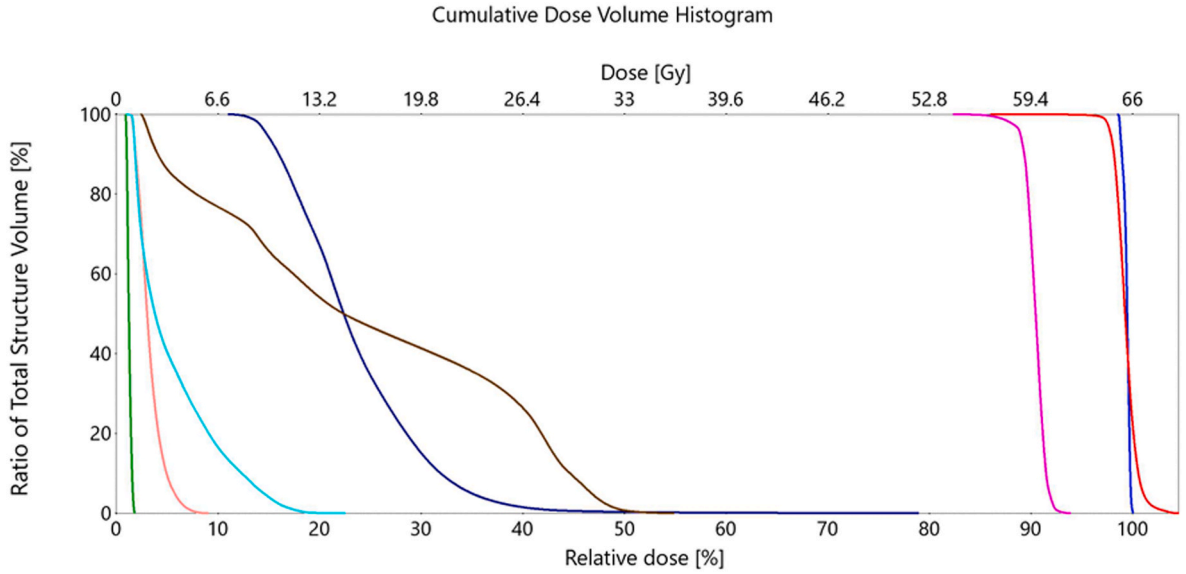

Fig. 2a. Cumulative Dose Volume Histogram of TPS generated IMRT plan to deliver 66Gy to a detector contoured as PTV high inside G-GAAB gel.

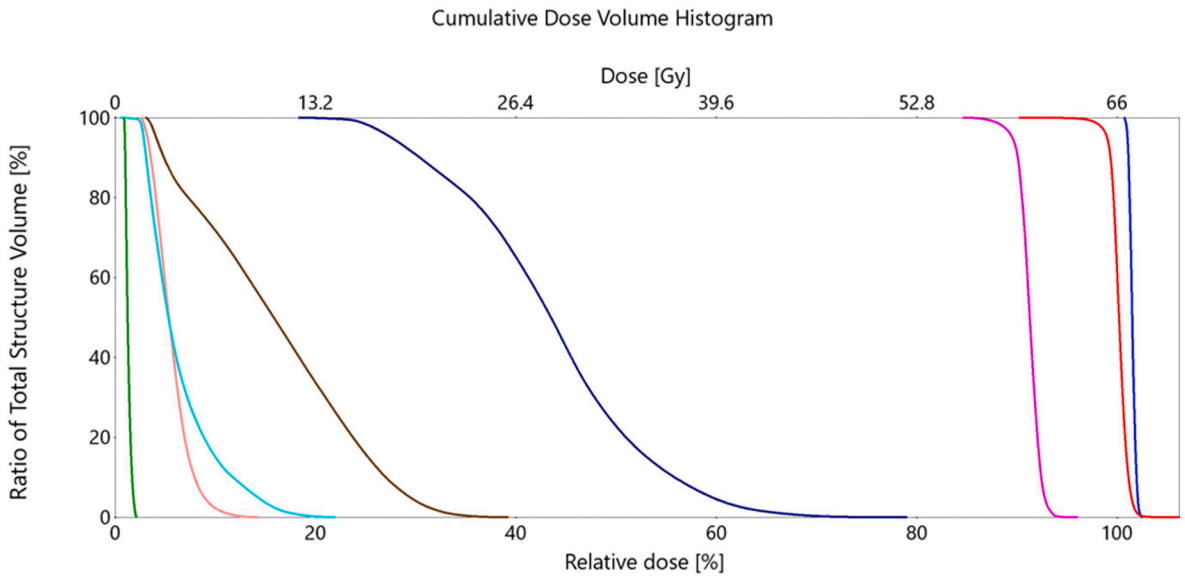

Fig. 2b. Cumulative Dose Volume Histogram of TPS generated VMAT plan to deliver 66Gy to a detector contoured as PTV high inside G-GAAB gel.

Table 5
Comparison of non-coplanar point dose calculated using TPS plan and measured in G-GAAB gel using 3DCRT, IMRT and VMAT techniques by 6MV photons when delivered with a dose of 5Gy.

Detector	3DCRT (Dose delivered - 5Gy)			IMRT (Dose delivered - 5Gy)			VMAT (Dose delivered - 5Gy)		
	TPS calculated dose (Gy)	Experimentally Measured dose (Gy)	% Deviation	TPS calculated dose (Gy)	Experimentally Measured dose (Gy)	% Deviation	TPS calculated dose (Gy)	Experimentally Measured dose (Gy)	% Deviation
0.6cc FC (PTW)	4.997	4.961	−0.72%	5.022	5.048	0.52%	5.043	5.056	0.26%
0.65cc FC (Rosalina)	6.155	6.203	0.78%	1.125	1.11	−1.33%	2.479	2.458	−0.85%
Semiflex 1 (PTW)	4.877	4.957	1.64%	4.979	4.93	−0.98%	4.563	4.499	−1.4%
Semiflex 2 (PTW)	5.935	6.005	1.18%	0.156	0.158	1.28%	0.079	0.0781	−1.14%
Pin point (PTW)	6.291	6.37	1.26%	1.279	1.259	−1.56%	1.706	1.736	1.76%
micro silicon (PTW)	5.532	5.486	−0.83%	0.127	0.125	−1.58%	0.129	0.127	−1.55%
Diode P (PTW)	4.476	4.399	−1.72%	0.0818	0.0811	−0.86%	0.093	0.094	1.08%
	P-value = 0.965		SD = 1.296	P-value = 0.994		SD = 1.111	P-value = 0.996		SD = 1.304

Table 6
Comparison of percentage dose deviations of point dose measurements for all three techniques (3DCRT, IMRT & VMAT) and detectors.

Detector	3DCRT (% Deviation)	IMRT (% Deviation)	VMAT (% Deviation)
0.6cc FC (PTW)	−0.72%	0.52%	0.26%
0.65cc FC (Rosalina)	0.78%	−1.33%	−0.85%
Semiflex 1 (PTW)	1.64%	−0.98%	−1.4%
Semiflex 2 (PTW)	1.18%	1.28%	−1.14%
Pin point (PTW)	1.26%	−1.56%	1.76%
micro silicon (PTW)	−0.83%	−1.58%	−1.55%
Diode P (PTW)	−1.72%	−0.86%	1.08%
	SD = 1.296	SD = 1.111	SD = 1.304

deviation of 0.52%, and for VMAT, the doses were 5.043Gy (TPS) and 5.056Gy (measured), with a deviation of 0.26%. The measured doses from the delivered plans across all chambers in multiple planes showed good agreement with the TPS-calculated doses, with percentage deviations below 2%. The standard deviations of percentage variations in point doses were 1.296 for 3DCRT, 1.111 for IMRT, and 1.304 for VMAT. The corresponding p-values for dose measurements were 0.965 (3DCRT), 0.994 (IMRT), and 0.996 (VMAT), indicating no statistically significant differences. Additionally, the Mean Absolute Deviation in all cases was found to be less than 1%.

Based on established QA guidelines (IAEA TRS 430, AAPM TG 53), clinically acceptable deviations between TPS-calculated and measured doses should be within 3%. Based on the clinical experience and failure mode analysis, institutions define specific tolerance limits. In our institution, a 3% limit is followed. In this study, the deviation between TPS-calculated and experimentally measured doses was consistently below 2%, indicating precise and accurate radiation delivery. This level of agreement is especially critical for intracranial treatments, where minimizing dose deviations ensures accurate tumour targeting while sparing surrounding healthy tissue. The <2% deviation achieved in this study demonstrates the reliability of patient-specific QA using the G-GAAB gel phantom, supporting its suitability as an effective tool for non-coplanar dose verification in radiotherapy.

For statistical analysis in this study, Student's *t*-test (two-sample assuming equal variances) was employed to compare the dose values obtained from two independent groups: the TPS-calculated doses and the experimentally measured doses in the G-GAAB gel phantom for each treatment technique (3DCRT, IMRT, and VMAT). The primary objective was to evaluate whether the observed differences between these two groups were statistically significant or attributable to random variations. Student's *t*-test is widely used for comparing mean values between two independent datasets, especially when the sample size is moderate and variances are assumed to be similar. Since our comparisons involved independent, normally distributed data with reasonably homogeneous variance (TPS dose calculations and experimental dose measurements), the two-sample *t*-test assuming equal variances was considered appropriate. The statistical analysis was performed using Microsoft Excel, utilizing its built-in *t*-test function for two samples with equal variances. This approach provided reliable P-values to determine statistical significance and assess the agreement between the TPS-calculated and experimentally measured doses. Selection of this test ensured that the comparison was both statistically robust and relevant for validating the dosimetric accuracy of the G-GAAB gel phantom for PSQA applications.

The point dose measurements at multiple planes within the G-GAAB gel demonstrated no significant variation between the TPS-calculated and experimentally measured doses across all treatment techniques. This consistency confirms the uniform density of the G-GAAB gel and its radiation attenuation properties closely matching those of brain tissue.

3.3. PSQA- EPID and portal dosimetry-GI evaluation

The verification plans for both IMRT and VMAT were approved and executed on the Linac using 6MV X-rays. Images of the G-GAAB gel phantom irradiated with high-energy 6MV photons were captured using the EPID. For the IMRT plan, seven portal images were acquired corresponding to each of the seven beam angles, while two images were obtained for the two full arcs of the VMAT plan. All images were verified and analysed using the portal dosimetry system in Eclipse TPS. Each IMRT beam was individually analysed to ensure that the gamma index evaluation met the specified tolerance criteria. Subsequently, the seven individual IMRT images were combined into a composite image for comprehensive analysis. Similar analysis was carried out for the two arc images and the composite image of the VMAT plan. The histogram image of dose differences and gamma evaluations, along with their statistical distributions, are presented in Fig. 3a and b for IMRT and Fig. 4a and b for VMAT. The gamma index (GI) was analysed with gamma criteria of dose difference ≤3% and DTA ≤3mm for PSQA with a pass rate of area gamma ≥95% as the threshold for plan acceptability. Gamma index evaluation compared the planned and measured doses based on dose difference and distance to agreement. For IMRT plans with 6MV X-rays, the area gamma, maximum gamma, and average gamma values were 96.1%, 2.5, and 0.26, respectively, with a maximum dose difference of 0.92CU. For VMAT plans, the corresponding values were 98.9%, 2.72, and 0.15, with a maximum dose difference of 0.76CU. These illustrate that the majority of points within the G-GAAB gel phantom volume satisfied the dose difference <3% and distance-to-agreement <3mm (3%,3mm) criterion, with all evaluated plans achieving gamma pass rates exceeding 95%.

The results demonstrated that, within the G-GAAB gel phantom, the modulation of the radiation beams and dose distribution in the TPS plan closely matched the delivered dose. The absolute dose difference values exhibited a narrow distribution centered near zero for both IMRT and VMAT plans in the G-GAAB gel, indicating minimal variation between the planned and delivered doses. This confirmed that the planned and delivered doses were in good agreement and well within the tolerance limits. The results demonstrated that the complex radiation fluence patterns with varying intensities were accurately delivered in the G-GAAB gel phantom as planned using both IMRT and VMAT techniques.

3.4. Novel G-GAAB gel phantom for PSQA verification

Verification plans were created for 30 retrospective brain tumour cases using the G-GAAB gel phantom with three ionization chambers positioned in different planes within the gel. Both IMRT and VMAT plans were used for dose calculation. Point dose values were calculated at the locations of the ionization chambers in the TPS for each verification plan. The same procedure was also carried out using a solid slab phantom, and corresponding dose values were obtained for comparison.

The G-GAAB gel phantom, positioned with three different detectors and fiducial markers, was aligned with the treatment room lasers and irradiated with 6MV photon beams using a linear accelerator. A comparison between the planned doses from the TPS and the experimentally measured doses was performed for both the G-GAAB gel phantom and the conventional slab phantom. The percentage deviation between the planned and measured doses was calculated, and statistical analysis, including sample standard deviation and P-value, was conducted. The detailed results of this analysis are presented in Table 7.

In the G-GAAB gel phantom, the percentage deviation between the planned and measured doses ranged from −1.363% to 1.317% for the 0.6cc FC, −1.300% to 1.207% for the 0.65cc FC, and −1.530% to 1.402% for the Semiflex chamber. The corresponding standard deviations calculated for these chambers were 0.825, 0.803, and 0.889, respectively. P-values obtained from the statistical analysis of dose

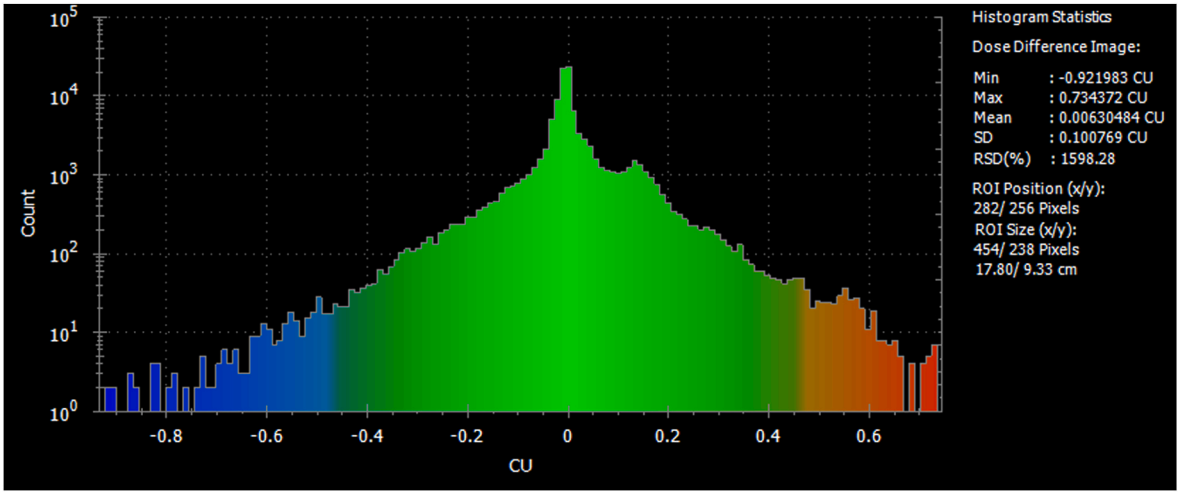

Fig. 3a. Histogram image of Dose difference with statistics for the gamma evaluation of IMRT plan delivered to G-GAAB gel.

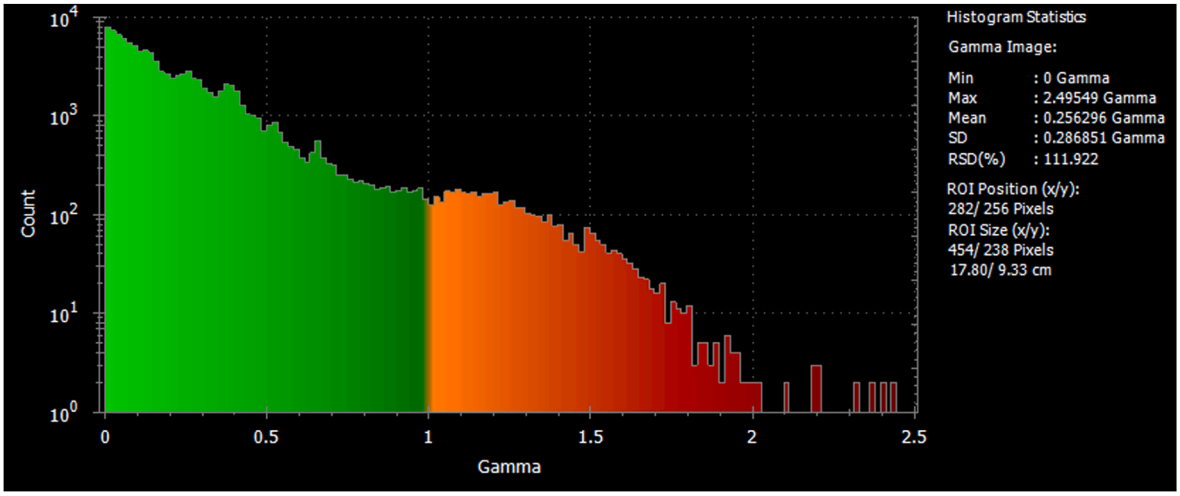

Fig. 3b. Histogram image of Gamma evaluation with statistics for the gamma evaluation of IMRT plan delivered to G-GAAB gel.

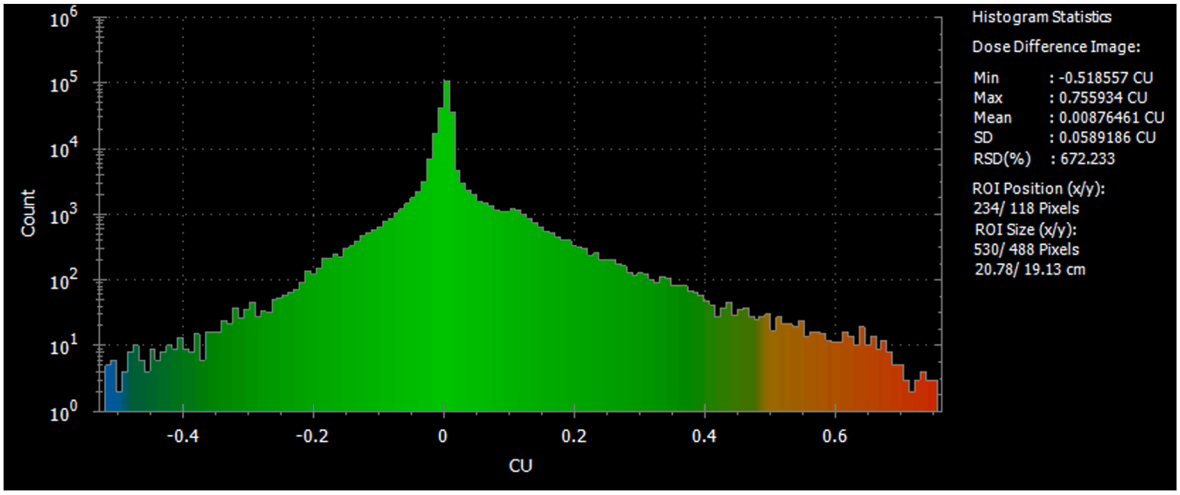

Fig. 4a. Histogram image of Dose difference with statistics for the gamma evaluation of VMAT plandelivered to G-GAAB gel.

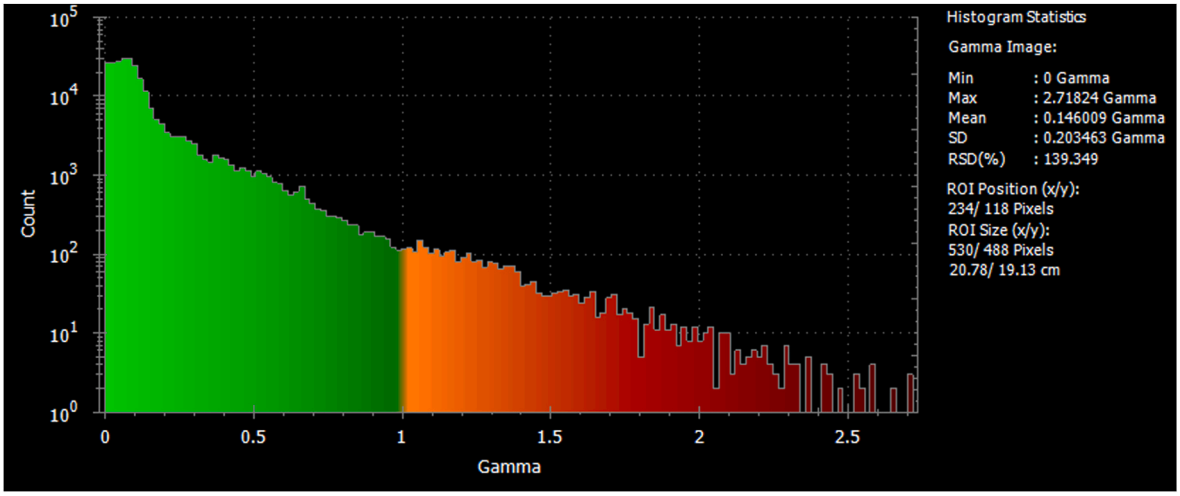

Fig. 4b. Histogram image of Gamma evaluation with statistics for the gamma evaluation of VMAT plan delivered to G-GAAB gel.

Table 7
Comparison of TPS-Calculated and measured absolute doses in G-GAAB gel and slab phantoms from 30 verification plans for PSQA.

Verification Plans	G-GAAB gel *positioned with 0.*6cc FC *(PTW)*			G-GAAB gel *positioned* with 0.65cc FC (Rosalina)			G-GAAB gel *positioned* with 0.07cc Semiflex chamber			Solid Slab Phantom *positioned with 0.*6cc FC *(PTW)*		
	TPS dose (Gy)	*Measured dose (Gy)*	% Deviation	*TPS dose (Gy)*	*Measured dose (Gy)*	% Deviation	*TPS dose (Gy)*	*Measured dose (Gy)*	% Deviation	*TPS dose (Gy)*	*Measured dose (Gy)*	% Deviation
1	2.132	2.116	−0.75%	1.861	1.848	−0.699%	0.775	0.767	−1.032%	1.964	1.99	1.324%
2	2.006	2.02	0.697%	2.034	2.028	−0.295%	1.369	1.357	−0.877%	1.925	1.89	−1.818%
3	1.905	1.903	−0.105%	1.585	1.602	1.072%	1.083	1.092	0.831%	1.813	1.786	−1.489%
4	1.906	1.904	−0.105%	2.021	1.996	−1.237%	0.713	0.723	1.402%	1.831	1.86	1.584%
5	2.054	2.07	0.779%	1.732	1.74	0.461%	1.116	1.109	−0.627%	1.916	1.93	0.731%
6	1.905	1.89	−0.787%	0.699	0.705	0.858%	0.292	0.289	−1.027%	1.711	1.695	−0.935%
7	1.807	1.799	−0.443%	1.801	1.79	−0.611%	1.229	1.219	−0.814%	1.726	1.756	1.738%
8	1.681	1.672	−0.535%	1.649	1.628	−1.273%	1.635	1.618	−1.04%	1.565	1.594	1.853%
9	1.813	1.832	1.048%	1.665	1.649	−0.961%	1.896	1.867	−1.53%	2.036	1.996	−1.965%
10	2.296	2.314	0.784%	2.801	2.798	−0.107%	0.587	0.591	0.681%	2.434	2.389	−1.849%
11	2.314	2.297	−0.735%	2.242	2.22	−0.981%	1.057	1.061	0.378%	2.14	2.15	0.467%
12	2.127	2.098	−1.363%	2.088	2.11	1.053%	1.348	1.333	−1.113%	1.895	1.92	1.319%
13	2.198	2.175	−1.046%	1.616	1.624	0.495%	2.315	2.299	−0.691%	2.12	2.08	−1.887%
14	2.039	2.026	−0.638%	2.005	1.987	−0.898%	1.192	1.204	1.006%	1.96	1.99	1.531%
15	1.83	1.806	−1.311%	0.879	0.886	0.796%	0.277	0.28	1.083%	1.684	1.659	−1.485%
Verification Plans	G-GAAB gel *positioned with 0.*6cc FC *(PTW)*			G-GAAB gel *positioned* with 0.65cc FC (Rosalina)			G-GAAB gel *positioned* with 0.07cc Semiflex chamber			Solid Slab Phantom *positioned with 0.*6cc FC *(PTW)*		
	TPS dose (Gy)	*Measured dose (Gy)*	% Deviation	*TPS dose (Gy)*	*Measured dose (Gy)*	% Deviation	*TPS dose (Gy)*	*Measured dose (Gy)*	% Deviation	*TPS dose (Gy)*	*Measured dose (Gy)*	% Deviation
16	1.891	1.91	1.004%	1.347	1.338	−0.668%	0.668	0.662	−0.898%	1.786	1.803	0.952%
17	2.024	2.037	0.642%	2.068	2.057	−0.532%	1.568	1.558	−0.638%	1.993	2.031	1.907%
18	1.883	1.871	−0.637%	1.941	1.939	−0.103%	1.090	1.1	0.917%	1.85	1.87	1.081%
19	1.847	1.837	−0.541%	1.513	1.498	−0.991%	0.965	0.958	−0.725%	1.743	1.723	−1.147%
20	2.049	2.07	1.024%	2.462	2.43	−1.3%	1.148	1.136	−1.045%	2.3	2.343	1.87%
21	1.925	1.907	−0.935%	2.018	2.03	0.595%	0.694	0.689	−0.72%	1.802	1.831	1.609%
22	2.041	2.056	0.735%	1.742	1.731	−0.631%	1.108	1.11	0.1805%	1.911	1.946	1.832%
23	1.899	1.924	1.317%	0.707	0.711	0.566%	0.33	0.328	−0.606%	1.699	1.666	−1.942%
24	1.803	1.795	−0.444%	1.831	1.814	−0.928%	1.234	1.245	0.8914%	1.732	1.758	1.501%
25	1.667	1.681	0.839%	1.599	1.607	0.500%	1.641	1.653	0.7313%	1.574	1.597	1.461%
26	1.822	1.843	1.152%	1.68	1.672	−0.476%	1.902	1.881	−1.104%	2.11	2.145	1.659%
27	2.041	2.027	−0.686%	2.004	1.999	−0.25%	1.201	1.203	0.1665%	2.012	1.974	−1.889%
28	1.829	1.819	−0.547%	0.868	0.871	0.346%	0.286	0.283	−1.049%	1.598	1.63	2.003%
29	1.889	1.879	−0.529%	1.326	1.342	1.207%	0.702	0.706	0.5698%	1.764	1.795	1.757%
30	2.004	2.011	0.349%	2.12	2.14	0.943%	1.627	1.645	1.1063%	1.999	2.034	1.751%
	P-value for TPS dose nd and measured dose = 0.975		SD = 0.825	P-value for TPS dose nd and measured dose = 0.976		SD = 0.803	P-value for TPS dose nd and measured dose = 0.984		SD = 0.889	P-value for TPS dose nd and measured dose = 0.881		SD = 1.554

readings inside the G-GAAB gel were 0.975 for the 0.6cc FC, 0.976 for the 0.65cc FC, and 0.984 for the Semiflex chamber, indicating no statistically significant difference between the planned and measured doses. In all three cases, the mean absolute deviation was negligibly small, confirming high consistency in dose agreement.

For the solid slab phantom, the percentage deviation measured using the 0.6cc FC ranged from −1.965% to 2.003%, with a standard deviation of 1.554 and a P-value of 0.881. A graphical representation comparing the spread of percentage deviations from the 0.6cc FC in both the G-GAAB gel and the slab phantom is shown in Fig. 5.

From the results, it was observed that the standard deviation calculated for percentage dose deviation across different ionization chambers arranged in non-coplanar positions within the G-GAAB gel, for 30 treatment plans, was less than one. Based on both the low standard deviation and the high P-values obtained, it was inferred that there was no significant difference between the TPS-calculated doses and the measured doses in the G-GAAB gel phantom. In comparison, the standard deviation of dose deviations in the solid slab phantom was 1.554. Although the P-values for the slab phantom also indicated no statistically significant difference, the comparison clearly showed that the G-GAAB gel exhibited consistently lower deviations, even across multiple planes and varied detector positions. This can be attributed to the inherent limitations of slab phantoms, where minor misalignments or air gaps between individual slabs during setup may introduce inconsistencies in dose calculations. In contrast, the G-GAAB gel provides a continuous, homogeneous medium without air gaps, ensuring uniform radiation interaction throughout its volume. Furthermore, the close match of G-GAAB gel to the physical, CT number, and radiation attenuation properties of brain tissue also contributed to the reduced dose deviations. Depth dose measurements in G-GAAB gel also showed a linear correlation with that in water, with a variation of less than 2% from previous studies. As a result, these characteristics contribute to the superior agreement observed between TPS-calculated and measured doses in G-GAAB gel, especially for non-coplanar and off-axis dose deliveries.

P-values from independent t-tests were obtained for dose readings of each ionization chamber positioned inside the G-GAAB gel, comparing TPS-calculated and experimentally measured doses across 30 plans. The P-values for the 0.6cc FC (PTW), 0.65cc FC (Rosalina), and Semiflex chamber (PTW) were 0.975, 0.976, and 0.984, respectively. Since all P-values were well above the conventional significance threshold of 0.05, it was inferred that there is no statistically significant difference between the planned and measured doses. This demonstrates a high level of agreement between TPS-calculated and experimentally measured dose values, confirming the suitability of the G-GAAB gel phantom for patient-specific QA applications.

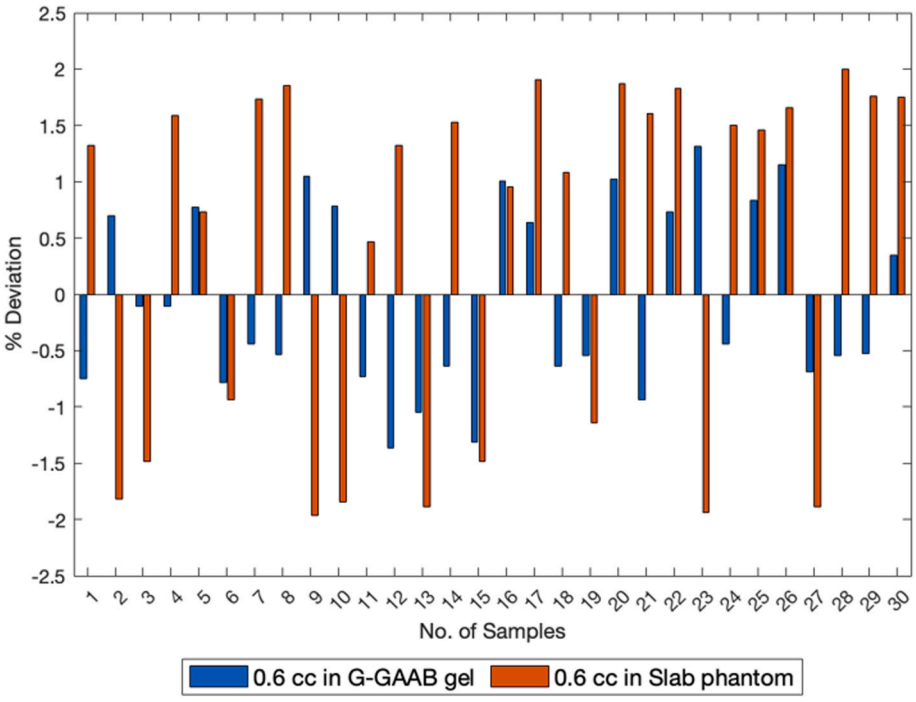

Fig. 5. Percentage deviation of dose values from 0.6cc FC in G-GAAB gel and 0.6cc FC in Slab phantom from 30 different brain tumour cases.

From the results obtained, it was understood that, the advantages of the G-GAAB gel phantom over conventional PSQA phantoms are noteworthy. Due to its liquid form during preparation, the G-GAAB gel can be poured and molded into any desired shape, with gelation occurring inside the mould to form a stable structure. Its gel nature allows the insertion of detectors at any depth, enabling flexible detector positioning which are not possible with traditional PSQA phantoms. Furthermore, it facilitates the placement of multiple detectors across various planes and orientations, which remains a challenge in conventional setups. This flexibility makes it particularly suitable for point dose measurements in non-coplanar geometries. The crosslinking of gelatin with gum arabic aldehyde provides excellent mechanical stability, ensuring that the detectors remain fixed during the measurement period without deformation or displacement.

The G-GAAB gel phantom closely replicates the tissue composition of the brain and enables point dose verification at any location within its volume, allowing effective quality assurance even in the presence of irregular tumour geometries and nearby critical structures. This capability enhances precision in dose delivery, which is particularly critical in brain tumour treatments, where even minor setup errors or dose uncertainties can lead to significant clinical consequences. Furthermore, being anatomically relevant and moldable into any desired shape, the G-GAAB gel provides a more realistic simulation of the actual brain compared to conventional slab or homogeneous rigid phantoms. The results obtained from non-coplanar dose measurements in this study demonstrate the suitability of the G-GAAB gel phantom for integration into clinical routine PSQA workflows. These features of the G-GAAB gel not only improve verification accuracy but also streamline the QA process by reducing effort and time. Unlike traditional PSQA phantoms that typically support only planar or limited volumetric verification, the G-GAAB gel phantom allows flexible detector positioning across multiple planes and orientations, thereby enabling accurate verification of complex non-coplanar treatment plans, particularly for advanced treatment techniques. These features collectively establish the G-GAAB gel phantom as a promising and reliable tool for patient-specific quality assurance in advanced radiotherapy techniques such as IMRT and VMAT.

In a previous study on the development and dosimetric evaluation of G-GAAB gel (T. Niju Thankachan et al., 2025), the material demonstrated superior brain-equivalent properties in terms of radiation attenuation, CT number, density, and overall dosimetric behaviour. It was also compared with water to assess its suitability as a tissue-equivalent material for broader dosimetric applications beyond brain studies. Using Phy-X software, the MAC values of the gel and water at 6MV were 0.0270cm^2/g and 0.0280cm^2/g, respectively, while at 15MV, the values were 0.0180cm^2/g and 0.0190cm^2/g, respectively. This close agreement in MAC values supports the G-GAAB gel's effectiveness as a tissue-equivalent material for photon beam attenuation studies. Furthermore, depth dose measurements performed in the G-GAAB gel phantom showed a linear correlation with those obtained in a water phantom (Radiation Field Analyser), with deviations of less than 2%, further validating its dosimetric equivalence to water. These results suggest that G-GAAB gel can reasonably simulate soft tissues with attenuation properties similar to water, making it suitable for dosimetric studies of various soft tissues beyond brain, particularly in radiation therapy.

The primary challenge encountered during the initial setup was ensuring the accurate positioning of detectors within the gel phantom. Although the G-GAAB gel exhibited good mechanical stability, achieving precise perpendicular alignment of the detectors with respect to the beam axis proved difficult and required multiple adjustments. Occasional minor tilting of the detectors was observed, particularly while connecting the detector cables to the electrometer. To mitigate this, once proper alignment was achieved, careful measures were taken to avoid any disturbance to the setup, including minimizing movement of the detector cables. Overall, detector alignment remained the most critical challenge during the experimental procedure.

The G-GAAB gel phantom exhibited excellent stability throughout the duration of this study. However, certain limitations were noted regarding temperature control and shelf life beyond one month. No noticeable degradation or deformation was observed within the one-month period of preparation and experimentation, but further studies are required to evaluate its stability under varying temperature conditions to ensure long-term preservation of the gel structure. Future work should also focus on optimizing the formulation, particularly by increasing the concentration of the cross-linking agent, to further

enhance the mechanical stability and extend the shelf life of the G-GAAB gel phantom.

As future perspective, studies will be conducted to explore the feasibility of using G-GAAB gel as a gel dosimeter. Studies will also focus on evaluating the angular and energy dependence of various detectors embedded within the G-GAAB gel. Additionally, the response of the gel material to different dose rates in various radiation modalities, including proton and electron beams, will be investigated. Specific emphasis will be placed on electron beam dosimetry to assess the radiological equivalence of G-GAAB gel to brain tissue. Given its volumetric nature, the phantom could also serve as a valuable tool for precise dosimetric studies in proton therapy, particularly in regions of sharp dose gradients such as the Bragg peak. Further research will aim to improve the mechanical strength and stability of the gel for extended shelf life under varying temperature conditions. Moreover, studies on optimizing the degree of oxidation of gum arabic aldehyde for enhanced cross-linking will be carried out to increase the rigidity and long-term stability of the gel.

4. Conclusion

This study demonstrated the development and evaluation of a novel PSQA brain phantom using G-GAAB gel for accurate dose verification in advanced radiotherapy techniques such as IMRT and VMAT, particularly for non-coplanar dose deliveries. The phantom, embedded with detectors contoured as PTV and OARs, demonstrated excellent agreement between planned and measured doses. Plan evaluation demonstrated through Isodose distributions confirmed that 100% of the GTV and 95% of the PTV received the prescribed dose across both IMRT and VMAT plans. All OARs remained within dose constraints.

DVH analysis indicated that, the maximum doses for the IMRT and VMAT plans were 104.5% and 106.2%, respectively and both within the acceptable limit of 107%. The volumes receiving 95% of the prescribed dose were 76.033cm^3 for IMRT and 76.076cm^3 for VMAT, closely matching the PTV volume of 76.13cm^3. The calculated CI values were 0.9987 for IMRT and 0.9992 for VMAT, indicating excellent dose conformity. The corresponding HI values were 0.0439 (IMRT) and 0.0344 (VMAT), demonstrating high dose uniformity. With CI values near 1 and HI values close to zero, both IMRT and VMAT plans showed excellent conformity and homogeneity of dose distribution within the G-GAAB gel phantom.

Non-coplanar point dose measurements confirmed good agreement between TPS-calculated and experimentally measured doses. For a prescribed dose of 5Gy using the 3DCRT technique, the dose recorded by the 0.6 cc FC was 4.997Gy in the TPS plan and 4.961Gy from the experimental measurement, corresponding to a deviation of −0.72 %. Similarly, for IMRT, the dose received by the 0.6 cc FC was 5.022Gy in the calculated plan and 5.048Gy from experimental measurement, with a deviation of 0.52%. For the VMAT plan, the respective TPS and measured doses were 5.043Gy and 5.056Gy, yielding a deviation of 0.26%.

The doses measured using the Linac for all detectors placed in multiple planes closely matched the TPS-calculated doses, with percentage deviations below 2%. Non-coplanar point dose measurements, along with low standard deviation and high P-values, showed no statistically significant difference between the calculated and delivered doses, regardless of the treatment technique. These results confirm that the G-GAAB gel has uniform density and consistent radiation attenuation properties, similar to those of soft tissues like the brain.

The PSQA results clearly demonstrated that the different dose levels prescribed to various regions within the G-GAAB gel were accurately calculated in the TPS-generated plans and subsequently verified through experimental measurements under clinical conditions. The Gamma Index analysis further confirmed that the modulation of the radiation beam and the resulting dose distribution in the TPS closely matched the delivered dose distribution well within the tolerance limit. For IMRT plans using 6MV X-rays, the area gamma, maximum gamma, and average gamma values were 96.1%, 2.5, and 0.26, respectively, with a maximum dose difference of 0.92CU. For VMAT plans, the corresponding values were 98.9%, 2.72, and 0.15, with a maximum dose difference of 0.76CU. These results indicate that the majority of points within the G-GAAB gel phantom satisfied the 3% dose difference and 3mm distance-to-agreement (3%, 3mm) gamma criteria, with all evaluated plans achieving pass rates above the clinically acceptable threshold of 95%. The absolute dose difference analysis showed a narrow distribution centered near zero for both IMRT and VMAT plans, indicating minimal variation between planned and delivered doses. This reflects a high level of agreement between the calculated and measured doses, well within clinically acceptable tolerance limits. These findings confirm that the complex radiation fluence patterns with varying intensities were delivered with high precision as planned in the G-GAAB gel using both IMRT and VMAT techniques.

From the dose comparison results of verification plans for 30 different retrospective brain tumour cases, it was observed that the standard deviation of percentage dose deviation across multiple ionization chambers arranged in non-coplanar positions within the G-GAAB gel was less than one. Based on the low standard deviation and high P-values obtained, it was inferred that there was no significant difference between the doses calculated from the TPS verification plans and those measured from the delivered plans in the G-GAAB gel.

Although the standard deviation and P-value of dose measurements in the solid slab phantom also indicated no statistically significant difference between the TPS-calculated and measured doses, a comparative analysis revealed that the G-GAAB gel exhibited significantly lower dose deviations. This negligible deviation in G-GAAB gel was consistent across multiple planes and positions, demonstrating its superior dosimetric accuracy over the conventional slab phantom. This can be attributed to the inherent limitations of slab phantoms, where minor misalignments or air gaps between individual slabs during setup may introduce inconsistencies in dose calculations. In contrast, the G-GAAB gel provides a continuous, homogeneous medium, ensuring uniform radiation interaction throughout its volume similar to that of brain tissue.

Most commercially available PSQA phantoms are often limited by fixed detector placements at fixed or central positions. Even in models with multiple detector positions, the locations are predetermined and limited to specific points within the phantom. The development of the G-GAAB gel phantom represents a significant advancement in PSQA for advanced radiotherapy techniques. Unlike rigid or slab phantoms, the G-GAAB gel phantom combines anatomical relevance, tissue-equivalent radiological properties, and customizable geometry. Due to its liquid form during preparation, the G-GAAB gel can be poured and molded into any desired shape, with gelation occurring inside the mould to form a stable structure. Its gel-based structure and moldable nature allows detectors to be positioned at any depth, location, or orientation even in non-coplanar setups. This flexibility enables comprehensive, end-to-end verification of complex treatment plans like IMRT and VMAT with greater anatomical realism. Clinically, this is particularly valuable for brain tumour treatments, where even minor dose inaccuracies can have serious implications. By realistically simulating tumour geometries and facilitating accurate dose verification, the G-GAAB gel phantom addresses the critical limitation of existing PSQA methods. Moreover, the ability to directly place detectors at clinically relevant positions eliminates the need for multiple phantom setups or repositioning. These features of the G-GAAB gel not only improve verification accuracy but also streamline the QA process by reducing effort and time. Its versatility to replicate actual treatment scenarios further enhances the precision, efficiency, and safety of advanced radiotherapy workflows. Additionally, Gafchromic films can also be embedded at any plane within the gel for dose distribution analysis.

In summary, the G-GAAB gel phantom represents a novel and clinically significant advancement in PSQA for advanced radiotherapy. Its

moldable nature, tissue-equivalent structure, ability to accommodate multiple detectors in any orientation and superior dosimetric accuracy set it apart from conventional commercial phantoms. By enabling precise, non-coplanar dose verification with enhanced anatomical realism, the G-GAAB gel offers a practical, cost-effective solution to improve the accuracy, efficiency, and safety of radiotherapy QA, particularly in complex brain treatments and also streamline the QA process by reducing effort and time.

Future studies will explore the feasibility of using G-GAAB gel as a gel dosimeter, focusing on its angular, energy, and dose rate dependence with various detectors. Further work will also evaluate its performance in electron and proton beam dosimetry, particularly near sharp dose gradients, while optimizing the gel's mechanical strength and stability for long-term use.

CRediT authorship contribution statement

Niju Thankachan T: Writing – original draft, Visualization, Validation, Software, Resources, Methodology, Investigation, Formal analysis, Data curation, Conceptualization. **Sreelakshmi K.:** Methodology, Investigation, Formal analysis, Data curation, Conceptualization. **Nirmala R. James:** Writing – review & editing, Visualization, Validation, Resources, Methodology, Investigation, Formal analysis, Conceptualization. **Jojo P. John:** Writing – review & editing, Visualization, Validation, Software, Methodology, Investigation, Formal analysis, Data curation, Conceptualization. **B.R. Bijini:** Writing – review & editing, Visualization, Validation, Supervision, Resources, Project administration, Methodology, Investigation, Formal analysis, Data curation, Conceptualization.

Declaration of competing interest

The authors declare that, they have no known competing financial interests or personal relationships that could have appeared to influence the work reported in this paper.

Acknowledgement

The authors express sincere gratitude to the Principal, Government Medical College, Thiruvananthapuram and Director, Indian Institute of Space Science and Technology, Kerala for providing facilities for conducting this study and first author is thankful for the devoted support of Ramya P R.

Data availability

Data will be made available on request.

References

Agazaryan, N., Solberg, T.D., DeMarco, J.J., 2003. Patient specific quality assurance for the delivery of intensity modulated radiotherapy. J. Appl. Clin. Med. Phys. 4 (1), 40–50. https://doi.org/10.1120/jacmp.v4i1.2540.

Breedveld, Sebastiaan, Craft, David, van Haveren, Rens, Heijmen, Ben, 2019. Multi-criteria optimization and decision-making in radiotherapy. Eur. J. Oper. Res. 277 (1), 1–19. https://doi.org/10.1016/j.ejor.2018.08.019. ISSN 0377-2217.

Devic, Slobodan, 2011. Radiochromic film dosimetry: past, present, and future. Phys. Med. 27 (3), 122–134. https://doi.org/10.1016/j.ejmp.2010.10.001. ISSN 1120-1797.

Drzymala, R.E., Mohan, R., Brewster, L., Chu, J., Goitein, M., Harms, W., Urie, M., 1991. Dose-volume histograms. Int. J. Radiat. Oncol. Biol. Phys. 21 (1), 71–78. https://doi.org/10.1016/0360-3016(91)90168-4.

Ferreira, C.C., Ximenes Filho, R.E.M., Vieira, J.W., Tomal, A., Poletti, M.E., Garcia, C.A. B., Maia, A.F., 2010. Evaluation of tissue-equivalent materials to be used as human brain tissue substitute in dosimetry for diagnostic radiology. Nucl. Instrum. Methods Phys. Res. Sect. B Beam Interact. Mater. Atoms 268 (16), 2515–2521. https://doi.org/10.1016/j.nimb.2010.05.051.

Fisher, R., Hintenlang, D., 2006. SU-FF-I-26: tissue equivalent phantoms for the evaluation of tube current modulated CT dose and image quality. Med. Phys. 33. https://doi.org/10.1118/1.2240265, 2002-2002.

Forte, A.E., Galvan, S., Manieri, F., Rodriguez y Baena, F., Dini, D., 2016. A composite hydrogel for brain tissue phantoms. Mater. Des. 112, 227–238. https://doi.org/10.1016/j.matdes.2016.09.063.

Goodwin, D., 2017. Point Dose Measurements in VMAT: an Investigation of Detector Choice and Plan Complexity.

Grech, N., Dalli, T., Mizzi, S., Meilak, L., Calleja, N., Zrinzo, A., 2020. Rising incidence of glioblastoma multiforme in a well-defined population. Cureus 12 (5), e8195. https://doi.org/10.7759/cureus.8195.

Hernandez, Victor, Hansen, Christian Rønn, Widesott, Lamberto, Bäck, Anna, Canters, Richard, Fusella, Marco, Götstedt, Julia, Jurado-Bruggeman, Diego, Mukumoto, Nobutaka, Kaplan, Laura Patricia, Koniarová, Irena, Piotrowski, Tomasz, Placidi, Lorenzo, Vaniqui, Ana, Jornet, Nuria, 2020. What is plan quality in radiotherapy? The importance of evaluating dose metrics, complexity, and robustness of treatment plans. Radiother. Oncol. 153, 26–33. https://doi.org/10.1016/j.radonc.2020.09.038. ISSN 0167-8140.

Ilic, I., Ilic, M., 2023. International patterns and trends in the brain cancer incidence and mortality:an observational study based on the global burden of disease. Heliyon 9 (7), e18222. https://doi.org/10.1016/j.heliyon.2023.e18222.

International Atomic Energy Agency, 2023. *Dosimetry of Small Static Fields Used in External Beam Radiotherapy: an International Code of Practice for Reference and Relative Dose Determination* (Technical Reports Series No. 398, Rev. 1). IAEA. https://www.iaea.org/publications.

James, Shands, Basheer, Al, Ahmad, Elder, Eric, Huh, Chulhaeng, Ackerman, Christopher, Barrett, John, Hamilton, Russell, Mostafaei, Farshad, 2023. Evaluation of commercial devices for patient specific QA of stereotactic radiotherapy plans. J. Appl. Clin. Med. Phys. 24, e14009. https://doi.org/10.1002/acm2.14009.

Kataria, T., Sharma, K., Subramani, V., Karrthick, K.P., Bisht, S.S., 2012. Homogeneity index: an objective tool for assessment of conformal radiation treatments. J. Med. Phys. 37 (4), 207–213. https://doi.org/10.4103/0971-6203.103606.

Khan, F.M., Gibbons, J.P., 2014. Khan's the Physics of Radiation Therapy. Lippincott Williams & Wilkins.

Knöös, T., Kristensen, I., Nilsson, P., 1998. Volumetric and dosimetric evaluation of radiation treatment plans: radiation conformity index. Int. J. Radiat. Oncol. Biol. Phys. 42 (5), 1169–1176. https://doi.org/10.1016/s0360-3016(98)00239-9.

Krishnan, M.P.A., Momeen, M.U., 2024. Verifying institutionally developed hybrid 3D-printed coaxial cylindrical phantom for patient-specific quality assurance in stereotactic body radiation therapy of hepatocellular carcinoma. Radiol. Phys. Technol. 17, 230–237. https://doi.org/10.1007/s12194-023-00769-4.

Kruszyna-Mochalska, M., Skrobala, A., Romanski, P., Ryczkowski, A., Suchorska, W., Kulcenty, K., Piotrowski, I., Borowicz, D., Matuszak, N., Malicki, J., 2022. Development of a quasi-humanoid phantom to perform dosimetric and radiobiological measurements for out-of-field doses from external beam radiation therapy. J. Appl. Clin. Med. Phys. 23 (4), e13514. https://doi.org/10.1002/acm2.13514.

Kumar, A., Mukherjee, G., Yadav, G., Pandey, V., Bhattacharya, K., 2007. Optimized point dose measurement: an effective tool for QA in intensity-modulated radiotherapy. J. Med. Phys. 32 (4), 156. https://doi.org/10.4103/0971-6203.37480.

Kumar, Rajesh, Sharma, Drdk, Deshpande, Sudesh, Ghadi, Yogesh & v.S., Shaiju & Amols, H.I., Mayya, Yelia, 2009. Acrylonitrile butadiene styrene (ABS) plastic-based low cost tissue equivalent phantom for verification dosimetry in IMRT. J. Appl. Clin. Med. Phys./Am. Coll. Med. Phy. 11, 3030. https://doi.org/10.1120/jacmp.v11i1.3030.

Kyei, K.A., Daniels, J., Adom, A.K., Odonkor, P., Nyantakyi, A.Y., Adjabu, D.E., 2024. A dosimetric evaluation of intensity modulated radiotherapy and three-dimensional conformal radiotherapy for prostate cancer in Ghana. ecancermedicalscience 18. https://doi.org/10.3332/ecancer.2024.1707.

Low, D.A., Moran, J.M., Dempsey, J.F., Dong, L., Oldham, M., 2011. Dosimetry tools and techniques for IMRT. Med. Phys. 38 (3), 1313–1338. https://doi.org/10.1118/1.3514120.

Mahmood, T., Ibrahim, M., Aqeel, M., 2017. Uncertainty assessment: relative versus absolute point dose measurement for patient specific quality assurance in EBRT. Progre Med. Phys. 28 (3), 111. https://doi.org/10.14316/pmp.2017.28.3.111.

Mahur, M., Gurjar, O.P., Grover, R., Negi, P., Sharma, R., Singh, A., Singh, M., 2017. Evaluation of effect of different computed tomography scanning protocols on hounsfield unit and its impact on dose calculation by treatment planning system. Iranian J. Med. Phys. 14 (3), 149–154. https://doi.org/10.22038/ijmp.2017.21942.1207.

Marashdeh, M., Abdulkarim, M., 2023. Determination of the attenuation coefficients of epoxy resin with carbopol polymer as a breast phantom material at low photon energy range. Polymers 15 (12), 2645. https://doi.org/10.3390/polym15122645.

Menzel, H.G., 2010. The international commission on radiation units and measurements report 83. J. ICRU 10 (1), 1–106.

Miften, M., Olch, A., Mihailidis, D., Moran, J., Pawlicki, T., Molineu, A., Li, H., Wijesooriya, K., Shi, J., Xia, P., Papanikolaou, N., Low, D.A., 2018. Tolerance limits and methodologies for IMRT measurement-based verification QA: recommendations of AAPM task group no. 218. Med. Phys. 45 (4), e53–e83. https://doi.org/10.1002/mp.12810.

Miri, N., Keller, P., Zwan, B.J., Greer, P., 2016. EPID-Based dosimetry to verify IMRT planar dose distribution for the aS1200 EPID and FFF beams. J. Appl. Clin. Med. Phys. 17 (6), 292–304. https://doi.org/10.1120/jacmp.v17i6.6336.

Molineu, Andrea, Followill, David S., Balter, Peter A., Hanson, William F., Gillin, Michael T., Saiful Huq, M., Eisbruch, Avraham, Ibbott, Geoffrey S., 2005. Design and implementation of an anthropomorphic quality assurance phantom for intensity-modulated radiation therapy for the radiation therapy oncology group. Int. J. Radiat. Oncol. Biol. Phys. 63 (2), 577–583. https://doi.org/10.1016/j.ijrobp.2005.05.021. ISSN 0360-3016.

Nasseri, S., Bahreyni, M.H., Momennezhad, M., Gholamhosseinian, H., Shahedi, F., Hashemi, S.M., Mohammadi, M., 2022. Dosimetric verification of IMRT and 3D conformal treatment delivery using EPID. Appl. Radiat. Isot. 182, 110116. https://doi.org/10.1016/j.apradiso.2022.110116. ISSN 0969-8043.

Niju Thankachan, T., James, Nirmala R., John, Jojo P., Bijini, Development, B.R., 2025. Characterization and radiation dosimetry evaluation of bovine gelatin crosslinked with gum Arabic aldehyde as brain phantom gel material in radiation therapy. Radiat. Phys. Chem. 229, 112416. https://doi.org/10.1016/j.radphyschem.2024.112416. ISSN 0969-806X.

Nishiyama, S., Takemura, A., 2023. A method for patient-specific DVH verification using a high-sampling-rate log file in an elekta linac. J. Appl. Clin. Med. Phys. 24, e13849. https://doi.org/10.1002/acm2.13849.

Nur, Emirah Mohd Zain, Jais, Umairah, Abdullah, Reduan, Abdullah, Reduan, Rahman, Wan Nordiana Wan Abd, 2019. Dosimetric characterization of customized PLA phantom for radiotherapy. Jurnal Sains Nuklear Malaysia 31 (2), 1–6.

Paddick, I., 2000. A simple scoring ratio to index the conformity of radiosurgical treatment plans. Technical note. J. Neurosurg. 93 (Suppl. 3), 219–222. https://doi.org/10.3171/jns.2000.93.supplement.

Petrova, D., Smickovska, S., Lazarevska, E., 2017. Conformity index and homogeneity index of the postoperative whole breast radiotherapy. Open Access Macedonian J. Med. Sci. 5 (6), 736–739. https://doi.org/10.3889/oamjms.2017.161.

Prabhu, Srilakshmi, Bharadwaj, Dhanya, Podder, Rachaita, sg, Bubbly, Gudennavar, S., 2021. Natural polymer-based hydrogels as prospective tissue equivalent materials for radiation therapy and dosimetry. Phys. Eng. Sci. Med. 44. https://doi.org/10.1007/s13246-021-01047-6.

Rousseau, Alice, Stien, Christel, Gouriou, Jean, Bordy, Jean-Marc, Boissonnat, Guillaume, Chabert, Isabelle, Dufreneix, Stephane, Blideanu, Valentin, 2023. End-to-end quality assurance for stereotactic radiotherapy with fricke-xylenol orange-Gelatin gel dosimeter and dual-wavelength cone-beam optical CT readout. Phys. Med. 113, 102656. https://doi.org/10.1016/j.ejmp.2023.102656.

Salam Abdulrazzaq Ibrahim Al-Rawi (physics) , Hassan Abouelenein (lecturer) , Magdy Mohammed Khalil (lecturer), 2022. Haidar hamza alabdei (lecturer) , awf abdulrahman sulaiman (radiotherapist) , dalya saad Al-Nuaimi (radiotherapist) , mohamed El-Sayed EL nagdy (lecturer) , evaluation of conformity and homogeneity indices consistency throughout the course of head and neck cancer treatment with and without using adaptive volumetric modulated arc radiotherapy CI and HI with and without adaptive VMAT in HNC. Adv. Radiat. Oncol. https://doi.org/10.1016/j.adro.2022.100905.

Sekkat, H., Khallouqi, A., Halimi, A., El rhazouani, O., 2025. Fabrication of new tissue equivalent materials as brain matter substitutes in diagnostic radiology. Mater. Lett. 382, 137920. https://doi.org/10.1016/j.matlet.2024.137920. ISSN0167-577X.

Shi, Mengying, Myronakis, Marios, Hu, Yue-Houng, Jacobson, Matthew, Lehmann, Mathias, Füglistaller, Rony, Huber, Pascal, Baturin, Paul, Wang, Adam, Ferguson, Dianne, Harris, Thomas, Morf, Daniel, Berbeco, Ross, 2019. A novel method for fast image simulation of flat panel detectors. Phys. Med. Biol. 64. https://doi.org/10.1088/1361-6560/ab12aa.

Sinead, M. Brennan, Thirion, Pierre, Buckney, Steve, Shea, Carmel O., Armstrong, John, 2010. Factors influencing conformity index in radiotherapy for non–small. Cell Lung Cancer 35 (1), 38–42. https://doi.org/10.1016/j.meddos.2009.01.003.

Singh, S., Raina, Payal, Gurjar, O.P., 2019. Point dose measurement for verification of treatment planning system using an Indigenous heterogeneous pelvis phantom for clarkson, convolution, superposition, and fast superposition algorithms. J. Biomed. Phys. Eng. 9. https://doi.org/10.31661/jbpe.v0i0.1185.

Thankachan, N., James, N.R., Jojo, P.J., Bijini, B.R, 2025. Experimental assessment of linear and mass attenuation coefficients of G-GAAB gel by narrow beam geometry with gamma rays and dual energy X-rays. Radiat. Phys. Chem. 237, 113143. https://doi.org/10.1016/j.radphyschem.2025.113143. ISSN 0969-806X.

Tino, R., Yeo, A., Leary, M., Brandt, M., Kron, T., 2019. A systematic review on 3D-Printed imaging and dosimetry phantoms in radiation therapy. Technol. Cancer Res. Treat. 18, 1533033819870208. https://doi.org/10.1177/1533033819870208.

Visser, R., Wauben, D.J., de Groot, M., Steenbakkers, R.J., Bijl, H.P., Godart, J., van't Veld, A.A., Langendijk, J.A., Korevaar, E.W., 2014. Evaluation of DVH-Based treatment plan verification in addition to gamma passing rates for head and neck IMRT. Radiother. Oncol. : J. European Soc. Therapeutic Radiol. Oncol. 112 (3), 389–395. https://doi.org/10.1016/j.radonc.2014.08.002.

Ximenes, R.E., Silva, A., Balbino, D., Poletti, M.E., Maia, A.F., 2015. Development of an anthropomorphic head phantom using dolomite and polymethyl methacrylate for dosimetry in computed tomography. Radiat. Phys. Chem. 117, 203–208. https://doi.org/10.1016/j.radphyschem.2015.08.019.

Yohannes, I., Kolditz, D., Langner, O., Kalender, W.A., 2012. A formulation of tissue- and water-equivalent materials using the stoichiometric analysis method for CT-number calibration in radiotherapy treatment planning. Phys. Med. Biol. 57 (5), 1173. https://doi.org/10.1088/0031-9155/57/5/1173.